CrossMark

ADVANCES AND TRENDS IN ADVANCED OXIDATION PROCESSES

Photocatalytic reduction of Cr(VI) by char/TiO₂ composite photocatalyst: optimization and modeling using the response surface methodology (RSM)

M. Antonopoulou[1] · I. Chondrodimou[1] · F. Bairamis[2] · A. Giannakas[1] · I. Konstantinou[1,2]

Abstract The photocatalytic reduction of Cr(VI) using pyrolytic char/TiO₂ (PC/TiO₂) composite catalyst under simulated solar irradiation was studied. Response surface methodology (RSM) and experimental design were used for modeling the removal kinetics and for the optimization of operational parameters. RSM was developed by considering a central composite design with four input variable, i.e. catalyst concentration, initial concentration of Cr(VI), pH, and % (v/v) methanol concentration for assessing individual and interactive effects. A quadratic model was established as a functional relationship between four independent variables and the removal efficiency of Cr(VI). It was found that all selected variables have significant effect on Cr(VI) removal efficiency; however, the pH, the % concentration of methanol, and their interaction exhibited the major effects. Within the studied experimental ranges, the optimum conditions for maximum Cr(VI) removal efficiency (72.1 %) after 60 min of photocatalytic treatment were: catalyst concentration 55 mg L^{-1}, Cr(VI) concentration 20 mg L^{-1}, pH 4, and 5 % (v/v) methanol concentration. Under optimum conditions, Cr(VI) reductive removal followed pseudo-first-order kinetics, and nearly complete removal took place within 90 min. The results revealed the feasibility and the effectiveness of PC/TiO₂ as photocatalyst in reduction reactions due to their ability of e$^-$–h$^+$ pair separation increasing the transfer of the photogenerated e$^-$ to the catalyst's surface and thus the reduction of Cr(VI).

Keywords Pyrolytic char · Photocatalysis · Cr(VI) · Reduction · Response surface methodology

Introduction

Hexavalent chromium, Cr(VI), is one of the most frequent and toxic heavy metals presented in wastewaters from various industrial processes such as leather tanning, electroplating, textile dying, pigment production, wood preservation, and finishing of metals and plastics, among others (Jacobs and Testa 2004). Cr(VI) is highly soluble and mobile in aquatic environment as well as toxic to various organisms and microorganisms with potential carcinogenic and mutagenic properties (Hawley et al. 2004; Barrera-Díaz et al. 2012). Given that water pollution caused by Cr(VI) is of particular environmental concern, extensive scientific efforts have been devoted on the removal of Cr(VI) from water and wastewaters or its reduction to less toxic Cr(III) (Hawley et al. 2004; Owlad et al. 2008; Mukherjee et al. 2013).

Nowadays, photocatalytic technologies attract considerable interest, especially for the oxidation of various persistent and/or toxic organic pollutants from aquatic matrices (Konstantinou and Albanis 2003, 2004; Chong et al. 2010). On the other hand, reduction by semiconductor photocatalysts is becoming more and more attractive for the removal or recovery of metal cations dissolved in wastewater. In general, photocatalytic reductive treatment can convert the ionic species into their metallic solid forms and deposit them over the semiconductor surface or transform them in less toxic soluble

✉ M. Antonopoulou
   mantonop@upatras.gr

✉ I. Konstantinou
   iokonst@cc.uoi.gr

1   Department of Environmental and Natural Resources Management, University of Patras, 30100 Agrinio, Greece

2   Department of Chemistry, University of Ioannina, 45110 Ioannina, Greece

Springer

species (Yue et al. 2015). Heterogeneous photocatalysis has been reported as a promising method for reducing Cr(VI) to the less toxic Cr(III) in aqueous solutions, and numerous studies with diverse catalysts (Antonopoulou et al. 2012; Barrera-Díaz et al. 2012; Giannakas et al. 2013, 2016; Machado et al. 2014; Cheng et al. 2015) have been devoted in this issue.

TiO$_2$ has been the most widely applied photocatalyst but suffers from low efficiency due to electron–hole recombination and low response in solar light. Combining TiO$_2$ with carbonaceous nanomaterials is being increasingly investigated as a means to increase photocatalytic activity (Jiang et al. 2011; Shaham-Waldmann and Paz 2013; Wang et al. 2014; Fu et al. 2015). The enhanced activity is attributed to the so-called synergistic effect, e.g., the adsorbent may adsorb a large amount of pollutant, thus facilitating the proximity/reaction of pollutant with the TiO$_2$ surface where the photocatalytic degradation/removal of pollutant takes place, or by increasing the separation of photogenerated electron–hole pairs due to the increased electrical conductivity for the majority of carbonaceous substrates (Lim et al. 2011; Leary and Westwood 2011; Zhao et al. 2013a, b). Conventional carbonaceous materials such as activated carbon (AC), carbon black (CB), and emerging materials such as [60]-fullerene, graphene, carbon nanotubes have been used to enhance TiO$_2$ efficiency (Leary and Westwood 2011; Lim et al. 2011; Zhao et al. 2012, 2013a, b). However, up until recently, the use of pyrolytic chars from industrial (such as tire rubber, etc.) or agricultural by-products as carbonaceous catalyst and photocatalyst supports has been investigated in a lower extent (Makrigianni et al. 2015; Ma et al. 2015; Rezaee et al. 2014; Pi et al. 2015).

In our previous study (Makrigianni et al. 2015), pyrolytic char/TiO$_2$ (PC/TiO$_2$) composite photocatalytic materials have been prepared, characterized, and proved efficient photocatalysts for the oxidation of phenol. Based on the results obtained from the catalyst characterization and photocatalytic activity, it was showed that pyrolytic char matrix can act as a very efficient electron acceptor from TiO$_2$ particles under UV–Vis irradiation resulting in decreased electron–hole pair recombination. This property could be beneficial for extrapolating the applications of such materials in photocatalytic reduction reactions such as the photocatalytic removal of heavy metal ions, like Cr(VI).

As a result, the application of PC/TiO$_2$ composite photocatalyst for the photocatalytic reduction of Cr(VI) was investigated in the present study by means of operational parameter optimization and modeling using the response surface methodology (RSM). The main objectives of this study were (a) to assess the applicability of the PC/TiO$_2$ catalyst toward the removal of Cr(VI), (b) to investigate the effect of four parameters (catalyst's concentration, initial concentration of Cr(VI), pH, and % (v/v) concentration of methanol, added as a hole scavenger) on the total process efficiency, and (c) to

model and optimize the photocatalytic procedure by means of a central composite design and response surface methodology.

Experimental section

Materials

Pyrolytic char/TiO$_2$ composite with (% wt.) char/TiO$_2$ ratio set at 0.5/2 (named as 0.5/2 PC/TiO$_2$) was prepared based on a simple sol–gel impregnation method, as mentioned in our previous work (Makrigianni et al. 2015). X-ray diffraction (XRD) patterns were measured using a Brüker Advance D8 instrument; elemental analysis was performed by Perkin Elmer (2400 Series II) analyzer; surface area was determined by N$_2$ porosimetry (Quantachrome Autosorb-1 instrument), while the point of zero charge (pH$_{pzc}$) was determined by the mass titration technique, according to the method reported in Makrigianni et al. (2015). Main physicochemical properties of the catalyst include anatase TiO$_2$ crystal phase with particle size of 17 nm; band gap energy (E_g) = 3.24 eV; surface area 81.5 m^2 g^{-1}; pH$_{PZC}$ = 5.9; C, N, and O elemental analysis at 5.09, 0.90, and 93.33 %, respectively).

Cr(VI) in the form of potassium dichromate was purchased from Sigma-Aldrich. Methanol (LC grade) was purchased from Merck (Darmstadt, Germany). Durapore membrane hydrophilic PVDF (Polyvinylidene Fluoride) 0.45-μm filters were supplied by Millipore. Ultrapure water was obtained from a Millipore Waters Milli-Q water purification system.

Photocatalytic experiments

Photocatalytic experiments were carried out in a solar simulator apparatus Atlas Suntest XLS+ (Atlas, Germany) equipped with a xenon lamp (2.2 kW) and special filters in place to prevent the transmission of wavelengths below 290 nm. A constant irradiation intensity of 350 W m^{-2} measured by an internal radiometer was maintained throughout the experiments. Cr(VI) aqueous solutions (250 mL) and the appropriate amount of catalyst were transferred into a double-walled Pyrex glass UV reactor with a water circulation. The pH of solutions was adjusted by adding appropriate volumes of H$_2$SO$_4$ or NaOH aqueous solutions. The suspension was kept in the dark for 60 min under stirring, prior to illumination to reach Cr(VI) adsorption equilibrium onto semiconductor surface. Aliquots (3 mL) were withdrawn from the reactor at different time intervals and were filtered through 0.45-μm filters in order to remove the catalyst's particles before further analysis. The concentration of Cr(VI) was determined by the diphenylcarbazide colorimetric method measuring the absorbance at the wavelength of 540 nm using a UV–Vis spectrophotometer (Hitachi, U-2000). The activity of the used catalyst for five consecutive catalytic cycles was also investigated.

After each cycle, the catalyst was washed with ultrapure water (pH = 4) and dried at 110 °C.

Experimental design and data analysis

A rotatable central composite design (CCD) was adopted for the optimization of photocatalytic process and for evaluating the effect of four main operational factors, i.e., catalyst (PC/TiO$_2$) concentration (x_1), Cr(VI) initial concentration (x_2), pH (x_3), and % (v/v) methanol concentration (x_4) added as a hole scavenger. For the four variables considered ($n = 4$) and two levels (high (−1) and low (+1)), the total number of experiments was determined by the expression $2^n + 2n + 6 = 2^4$ (16 factorial points) + 2 × 4 (8 axial (star) points) + 6 (central points, replications) = 30, as shown in Table 1, presented with

Table 1 The four-factor central composite design matrix (independent variables and their actual and coded (in parenthesis) levels; catalyst concentration (C_{cat}) and Cr(VI) concentration, $C_{Cr(VI)}$ in mg L^{-1}) and the experimental results for Cr(IV) % removal

C_{cat} (x_1)	$C_{Cr(VI)}$ (x_2)	pH (x_3)	% v/v Methanol (x_4)	% Removal
70.0 (0)	22.5 (0)	6.0 (0)	3.5 (0)	28.7
50.0 (−1)	30.0 (+1)	4.0 (−1)	5.0 (+1)	67.5
50.0 (−1)	15.0 (−1)	8.0 (+1)	5.0 (+1)	10.7
90.0 (+1)	15.0 (−1)	4.0 (−1)	2.0 (−1)	19.2
70.0 (0)	22.5 (0)	6.0 (0)	6.5 (+α)	68.0
70.0 (0)	22.5 (0)	6.0 (0)	3.5 (0)	28.7
70.0 (0)	22.5 (0)	6.0 (0)	3.5 (0)	27.0
70.0 (0)	22.5 (0)	6.0 (0)	0.5 (−α)	11.0
90.0 (+1)	30.0 (+1)	8.0 (+1)	2.0 (−1)	8.5
50.0 (−1)	15.0 (−1)	4.0 (−1)	5.0 (+1)	77.0
70.0 (0)	22.5 (0)	6.0 (0)	3.5 (0)	30.0
110.0 (+α)	22.50 (0)	6.0 (0)	3.5 (0)	11.8
70.0 (0)	22.5 (0)	6.0 (0)	3.5 (0)	28.9
90.0 (+1)	30.0 (+1)	8.0 (+1)	5.0 (+1)	8.0
90.0 (+1)	15.0 (−1)	4.0 (−1)	5.0 (+1)	68.0
90.0 (+1)	30.0 (+1)	4.0 (−1)	5.0 (+1)	54.2
50.0 (−1)	30.0 (+1)	4.0 (−1)	2.0 (−1)	16.0
30.0 (−α)	22.5 (0)	6.0 (0)	3.5 (0)	17.0
90.0 (+1)	15.0 (−1)	8.0 (+1)	5.0 (+1)	12.3
90.0 (+1)	15.0 (−1)	8.0 (+1)	2.0 (−1)	6.7
70.00 (0)	22.5 (0)	6.0 (0)	3.5 (0)	27.5
70.00 (0)	37.5 (+α)	6.0 (0)	3.5 (0)	4.5
50.0 (−1)	15.0 (−1)	4.0 (−1)	2.0 (−1)	19.8
70.0 (0)	7.5 (−α)	6.0 (0)	3.5 (0)	10.0
90.0 (+1)	30.0 (+1)	4.0 (−1)	2.0 (−1)	10.0
50.00 (−1)	15.00 (−1)	8.0 (+1)	2.0 (−1)	1.2
70.00 (0)	22.50 (0)	10.0 (+α)	3.5 (0)	8.0
70.00 (0)	22.50 (0)	2.0 (−α)	3.5 (0)	75.0
50.00 (−1)	30.00 (+1)	8.0 (+1)	2.0 (−1)	7.7
50.00 (−1)	30.00 (+1)	8.0 (+1)	5.0 (+1)	14.5

actual and coded values at levels −α, −1, 0, +1, +α. Taking into consideration that typical concentrations of Cr(VI) in wastewaters of tannery, pigments, and plating industries were in the range of 0.5–50 mg L^{-1}, the concentration range from 7.5 (−α) to 37.5 (+α) mg L^{-1} was selected as a compromise between (i) a concentration approximating real wastewaters and (ii) the concentration which enables obtaining not very fast kinetics. In addition, low catalyst concentration range was selected to show the effectiveness of the process, while the addition of methanol at 0.5 (−α) to 6.5 % (+α) (v/v) simulates the concentration of organic compounds that could be found in wastewaters acting as hole scavengers. The efficiency of the process evaluated by determining Cr(VI) removal percentages after a fixed time (60 min) of reaction was considered as the response of the experimental design according to the following equation:

$$Y(\%) = \left[\frac{C_0 - C_t}{C_0} \right] \times 100 \tag{1}$$

where C_0 is the initial Cr(VI) concentration and C_t the concentration after 60 min of photocatalytic treatment.

A second-order (quadratic) polynomial equation was used to fit the experimental results of CCD as follows:

$$
\begin{aligned}
Y(\%) = {} & b_0 + b_1 x_1 + b_2 x_2 + b_3 x_3 + b_4 x_4 + b_{12} x_1 x_2 \\
& + b_{13} x_1 x_3 + b_{14} x_1 x_4 + b_{23} x_2 x_3 + b_{24} x_2 x_4 + b_{34} x_3 x_4 \\
& + b_{11} x_1^2 + b_{22} x_2^2 + b_{33} x_3^2 + b_{44} x_4^2
\end{aligned} \tag{2}
$$

where Y represents the response variable (Cr(VI) removal efficiency); x_1, x_2, x_3, and x_4 are the studied independent variables, i.e., the concentration of catalyst, the initial concentration of Cr(VI), pH of the solution, and the percent content of methanol, respectively; b_i, b_{ii}, and b_{ij} are the regression coefficients for linear, quadratic effects and the coefficients of the interaction parameters, respectively.

Model adequacy was checked through lack-of-fit test based on analysis of variance (ANOVA) and calculated F values (Fisher variation ratio) as well as by various diagnostic tests, which included graphic representation of predicted vs. experimental values, a normal probability plot of the studentized residuals to check the normality of the residuals, the plot of studentized residuals vs. predicted values to check for constant errors, externally studentized residuals to check for outlier values, and Box−Cox plot for power transformations (Antonopoulou and Konstantinou 2015). The accuracy and applicability of the proposed model from RSM were evaluated by the statistic F value, the coefficient of determination (R^2), and the adjusted coefficient of determination (R^2_{adj}) for the parameters studied. The

significance of all model coefficients was judged based on the probability value ($p < 0.05$) with 95 % confidence level. Three-dimensional response surface plots were drawn for the visualization of the interaction effects of the independent operational parameters on Cr(VI) removal. Finally, the optimization was performed on the basis of the desirability function to determine the optimal conditions for Cr(VI) removal. Numerical optimization was used to identify the specific point that maximizes the desirability function. The experimental design, statistical analysis, response surface plots, and optimization were performed using Design Expert V.7.1.5 (Stat-Ease Inc. 2008, MN, USA) software.

Results

Preliminary experiments

Preliminary adsorption and photolysis experiments were carried out, before the development of the experimental design (data not shown). Direct photolysis was resulted in negligible removal of Cr(VI). Similarly, dark experiments in the presence of 0.5/2 PC/TiO$_2$ led to 10 % Cr(VI) adsorption on catalyst's surface, after the establishment of the adsorption equilibrium within 60 min. Moreover, photocatalytic experiments of Cr(VI) in the presence and absence of methanol were conducted. As shown in Fig. 1, the photocatalytic reduction of Cr(VI) is a slow process leading only to 18 % removal after 240 min (pH = 2). On the other hand, the presence of MeOH, a well-established hole scavenger, inhibited efficiently the electron–hole recombination leading to enhanced reduction of Cr(VI).
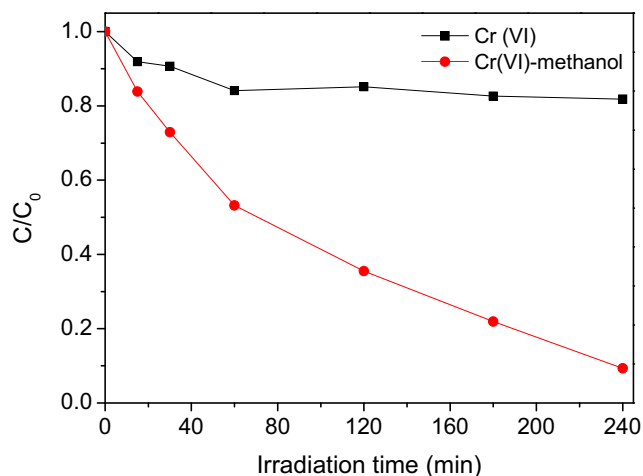

Fig. 1 Preliminary experiments of Cr(VI) photocatalytic reduction in the absence and presence of methanol ($C_{cat} = 100$ mg L^{-1}, $C_{Cr(VI)} = 20$ mg L^{-1}, pH = 2, % (v/v) methanol = 1 %)

RSM modeling and optimization for Cr(VI) photocatalytic removal

The experimental results obtained for Cr(VI) photocatalytic removal according to the CCD experiments are depicted in Table 1. Based on the experimental design, a quadratic response surface model was found to describe the empirical relationships between the independent variables and the response according to the following equation:

$$\%\text{Removal Cr(VI)} = 28.47 - 1.58x_1 - 1.65x_2 - 16.50x_3$$
$$+ 14.05x_4 - 1.41x_1x_2 + 1.89x_1x_3 - 1.68x_1x_4$$
$$+ 2.76x_2x_3 - 1.19x_2x_4 - 11.27x_3x_4$$
$$+ 3.61x_1^2 - 5.40x_2^2 + 3.16x_3^2 + 2.66x_4^2$$

$$(3)$$

The quadratic model developed for the prediction of Cr(VI) removal was initially evaluated for statistical significance using ANOVA, and the results are shown in Table 2.

The ANOVA results showed a p value <0.0001 and a high F value of 1176.72, indicating a highly significant model. There was only a 0.01 % chance that the "model F value" could occur due to noise. On the other hand, the lack-of-fit F value of 0.74 and the corresponding p value of 0.6825 indicated a non-significant shortage of the model in the prediction of experimental data.

The coefficient of determination (R^2) of the regression model is 0.9991, meaning that more than 99.91 % of the data deviation can be explained by the model. Similarly, the high value of adj. R^2 (0.9982) indicates a high degree of correlation between the experimental and predicted values and consequently a good predictability of the model.

Various diagnostic tests, i.e., the graphical representation of predicted vs. experimental (actual) values (Fig. 2a), the normal probability plot (Fig. 2b), the graphs of residual vs. predicted values (Fig. 2c), and the Box–Cox plot (Fig. 3) (Vaez et al. 2012; Antonopoulou and Konstantinou 2013) further verified the adequacy of the model.

Firstly, the good agreement between the experimental values (Y_{exp}) and the responses (Y_{cal}) predicted by the model (Fig. 2a) revealed the fitting capability of the suggested model. Secondly, the internally studentized residues in Fig. 2b lied reasonably close to the straight line indicating once more the adequacy of the model to describe the relationship between the studied variables and the response. Random dispersion of the residues and a distribution between −3 and +3 can also be seen in Fig. 2c. The good predictability of the model was finally confirmed by the Box–Cox plot (Fig. 3), as no transformation for the response is recommended (Chong et al. 2010).

Table 2 Analysis of variance (ANOVA) for response surface quadratic model applied for modeling Cr(VI) removal

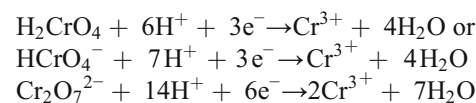| Source	Sum of squares	df	Mean square	F value	p value (Prob > F)
Model	15,572.60	14	1112.33	1176.72	<0.0001 (Significant)
A-C_{cat}	59.85	1	59.85	63.32	<0.0001
B-$C_{Cr(VI)}$	65.01	1	65.01	68.77	<0.0001
C-pH	6537.30	1	6537.30	6915.75	<0.0001
D-C_{MeOH}	4734.85	1	4734.85	5008.95	<0.0001
AB	31.64	1	31.64	33.47	<0.0001
AC	57.38	1	57.38	60.70	<0.0001
AD	45.23	1	45.23	47.84	<0.0001
BC	121.55	1	121.55	128.59	<0.0001
BD	22.80	1	22.80	24.12	0.0002
CD	2031.76	1	2031.76	2149.37	<0.0001
A^2	358.15	1	358.15	378.89	<0.0001
B^2	800.13	1	800.13	846.45	<0.0001
C^2	274.14	1	274.14	290.01	<0.0001
D^2	194.29	1	194.29	205.53	<0.0001
Residual	14.18	15	0.95		
Lack of fit	8.45	10	0.84	0.74	0.6825 (Not significant)
Pure error	5.73	5	1.15		
Cor total	15,586.77	29			

All the independent variables, their interaction effects, and the second-order effects are highly significant parameters with $p < 0.001$. Pareto analysis was used to estimate the effect of each variable on the photocatalytic removal of Cr(VI). The percentage effect of each factor on the response was calculated according to the following equation:

$$P_i = \left(\frac{\beta_i^2}{\sum \beta_i^2} \right) \qquad (4)$$

where β_i represent the regression coefficient for linear, quadratic, and interaction effects of the second-order polynomial response, Eq. 3 (Fathinia et al. 2010). According to Pareto graphic analysis depicted in Fig. 4, pH (40.1 %), % (v/v) methanol concentration (29.1 %), and their interaction (18.7 %) exhibited the highest effects on photocatalytic reduction efficiency. The sign of the coefficients in the obtained quadratic Eq. 3 indicates positive or negative effects (Antonopoulou and Konstantinou 2013). pH (x_3) presented the highest negative effects indicating that removal decreases as the values of the variable increases within the range studied. In contrast, % (v/v) methanol concentration (x_4) presented the highest positive effect implying that removal increases in the presence of high levels. Positive cross-product coefficients indicate a synergistic effect in the variation of parameters studied, while negative coefficients, an antagonistic effect. The highest synergistic effect was observed between Cr(VI) concentration (x_2) and pH (x_3), while the highest antagonistic effect was recorded between pH (x_3)

and % (v/v) methanol concentration (x_4). Negative quadratic term was obtained for Cr(VI) concentration (x_2) that corresponded to concave (negative curvature, dome-shaped) surfaces showing a higher removal efficiency at intermediate concentration levels of Cr(VI) within the range studied. On the other hand, positive quadratic terms were obtained for catalyst concentration (x_1), pH (x_3) and % (v/v) methanol concentration (x_4) that corresponded to convex (positive curvature, bowl-shaped) surfaces.

The effects of the four different operational parameters on Cr(VI) removal were visualized in three-dimensional response plots presented in Fig. 5a–d. As can be seen, there is an increase in the removal efficiency of Cr(VI) with an increase of PC/TiO$_2$ 0.5/2 concentration up to a certain concentration, above that the reaction rate levels off, and with a further increase, the removal started to decrease probably due to light scattering and screening effects at the given experimental conditions. The increase in pH leads to a decrease in the rate of Cr(VI) removal, as seen in Fig. 5a. For acidic pH in the range 2–6, the predominant species of Cr(VI) are $HCrO_4^-$ and $Cr_2O_7^{2-}$, while for pH values 2–3, $H_2Cr_2O_7$ contributes also by 0.5–5 % (Tandon et al. 1984), and the photocatalytic reaction of Cr(VI) occurred in the following way (Wang et al. 2009):

$$H_2CrO_4 + 6H^+ + 3e^- \rightarrow Cr^{3+} + 4H_2O \text{ or}$$
$$HCrO_4^- + 7H^+ + 3e^- \rightarrow Cr^{3+} + 4H_2O$$
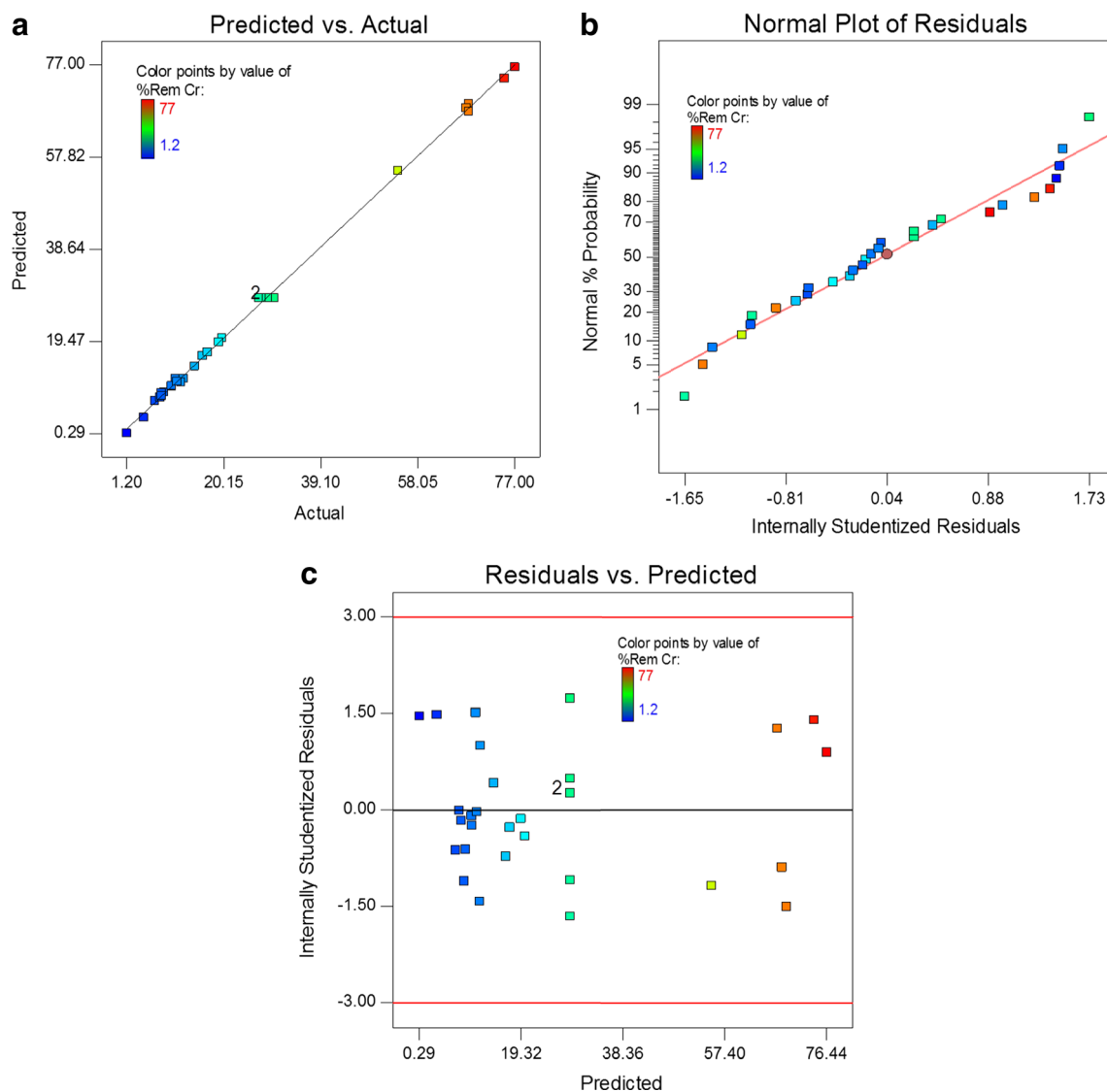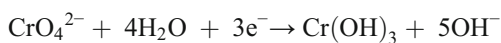$$Cr_2O_7^{2-} + 14H^+ + 6e^- \rightarrow 2Cr^{3+} + 7H_2O$$

Fig. 2 Residual diagnostics of quadratic model: **a** predicted vs. actual plot, **b** normal probability plot, and **c** internally studentized residuals vs. predicted values plot

As for alkaline medium, CrO_4^{2-} was the main species of Cr(VI), and the reaction proceeded as

$$CrO_4^{2-} + 4H_2O + 3e^- \rightarrow Cr(OH)_3 + 5OH^-$$

According to the above reactions, the photocatalytic reduction of Cr(VI) to Cr(III) consumes protons in acidic medium and produces hydroxyl anions in alkaline medium. Thereby, the reduction of Cr(VI) to Cr(III) is improved at acidic conditions and is inhibited at alkaline conditions according to Le Chatelier principle. The effect of pH on Cr(VI) reduction is assigned to the following three reasons. Firstly, the interactions (attraction or repulsion) between the surface charge of the PC/TiO_2 photocatalyst (PZC = 5.9) and the charge of Cr(VI) species in solution should be considered. As the pH of the solutions increases, the number of negatively charged

sites in PC/TiO_2 increases, and hence, the adsorption of Cr(VI) reduces due to electrostatic repulsion. On the other hand, at low pHs, the electrostatic attraction between the positively charged PC/TiO_2 surface and negatively charged Cr(VI) species is enhanced, thus increasing the reduction rates. The observed trends were also verified by the adsorbed percentages of Cr(VI) which were found to be 10 and 3 % in pH 4 and 8, respectively.

Secondly, the reduction product Cr(III) starts to precipitate in the catalyst surface in the form of $Cr(OH)_3$ at pH values higher than 5, so catalyst active sites are covered by the precipitates (Liu et al. 2014; Chen and Cao 2005) resulting to the decrease of the photocatalytic reduction efficiency.

Finally, the solution pH affects also the thermodynamic driving force for the photocatalytic reduction of Cr(VI), which is related with the potential difference between the Cr(VI)/
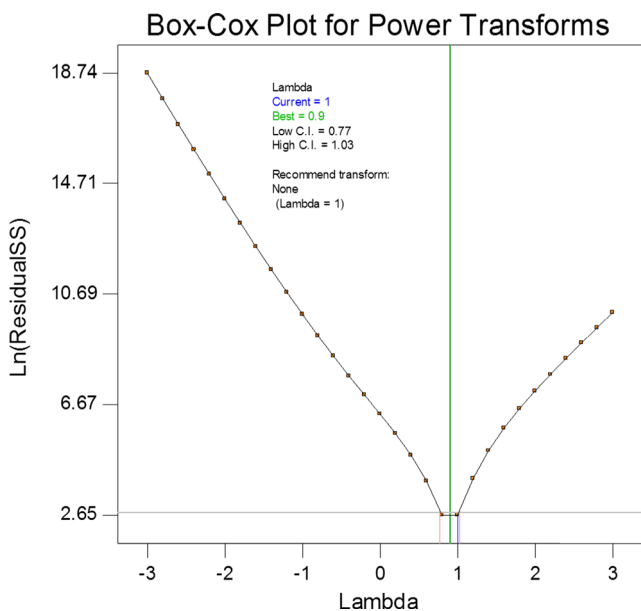
Fig. 3 Box–Cox plot showing optimized lambda for Cr(VI) photocatalytic removal efficiency

Cr(III) redox couple and electrons at the PC/TiO$_2$ conduction band (Zhao et al. 2013a, b). The reduction potential of Cr(VI) to Cr(III) is dependent on the solution pH, and the thermodynamic driving force decreases with increasing pH (Lin et al. 1993). The value of E^o [Cr(VI)/Cr(III)] varies with pH by −0.099 V/pH unit at 25 °C, so within the studied experimental range of pH 2–10 (−α, +α), E^o is decreased from 1.05 to 0.26 V. On the other hand, the energy level of TiO$_2$ conduction band varies with pH by −0.058 V/pH unit at 25 °C, thus within the experimental range of pH 2–10 (−α, +α) decreases from −0.17 to −0.63 V (Zhao et al. 2013a, b). As a result, the
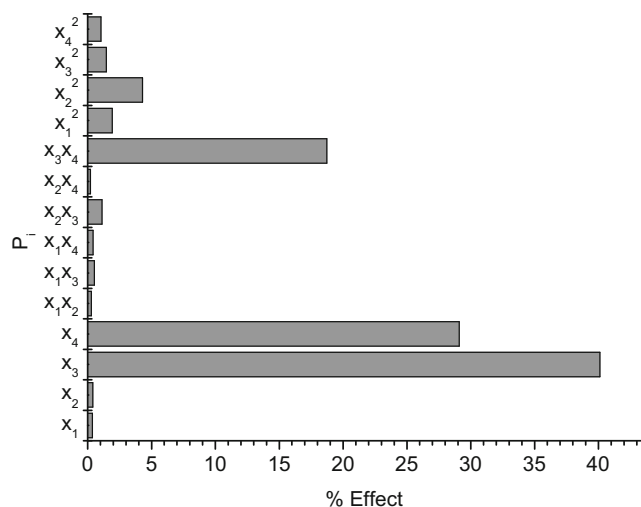

Fig. 4 Pareto graph analysis showing the relative effects of the first order, quadratic, and interaction terms of Eq. (3) on the photocatalytic reduction of Cr(VI). x_1, x_2, x_3, and x_4 are the studied variables, i.e., the concentration of catalyst, the initial concentration of Cr(VI), pH of the solution, and the percent content of methanol, respectively

potential difference that expresses the electron transfer dynamics decreases from 1.22 V at pH 2 to 0.89 V at pH 10, consequently the photocatalytic reduction of Cr(VI) is decreasing.

An increase in initial Cr(VI) concentration leads to a decrease percent removal, as the available photogenerated electrons become the limiting factor for Cr(VI) removal taking into consideration that the rate-determining step for the photocatalytic reduction of Cr(VI) is the surface reaction after Cr(VI) adsorption on TiO$_2$–carbon surface (Ku and Jung 2001). In addition, increased Cr(VI) concentration can provoke a "filter" effect on the available irradiation for catalyst excitation.

In contrast, increasing % (v/v) methanol concentration has a positive effect on the removal efficiency (Fig. 5d). This trend can be explained by the capability of methanol to act as an efficient scavenger of h$^+$ (Tan et al. 2003) inhibiting the recombination of electron–hole pairs. In addition, even though the methanol is moderately adsorbed, it has the ability to form reducing radicals via hydroxyl radicals or hole reaction resulting in the photoreduction of Cr(VI) ions in some extent (Tan et al. 2003).

The numerical optimization of the software using desirability approach was employed to find the specific points that maximize the % removal. The optimum conditions for the maximum removal efficiency were found as follows: catalyst concentration = 55 mg L^{-1}, initial concentration of Cr(VI) = 20 mg L^{-1}, methanol concentration = 5 % (v/v), and pH = 4.

Model validation and reusability of catalyst

To confirm the adequacy of the model for predicting the maximum % Cr(VI) removal, verification experiments were conducted using the optimum conditions. The removal kinetics from the validation experiment are depicted in Fig. 6. Under optimized conditions, first-order kinetics were recorded with a reaction rate constant of $k_{app} = 2.6 \times 10^{-2}$ min^{-1}, regression coefficient $R^2 = 0.9714$, and a half-life of 26.7 min. An average maximum removal of 72.1 % was obtained from three replicate experiments after 60 min, while the predicted removal value was 70.7 %. The good agreement (percent error was 1.9 %) between the predicted and the experimental removal values confirms the validity of the model for simulating Cr(VI) photocatalytic reduction. In addition, photocatalytic experiments under the optimum conditions using Degussa-P25 catalyst were also conducted for comparison, and the kinetic profile is depicted in Fig. 6. According to the kinetic data, P25-TiO$_2$ presented lower reduction activity than the prepared PC/TiO$_2$.

As the stability of catalysts is of great importance, the recycling use of PC/TiO$_2$ for removal of Cr(VI) was evaluated, and the results are shown in Fig. 7. It
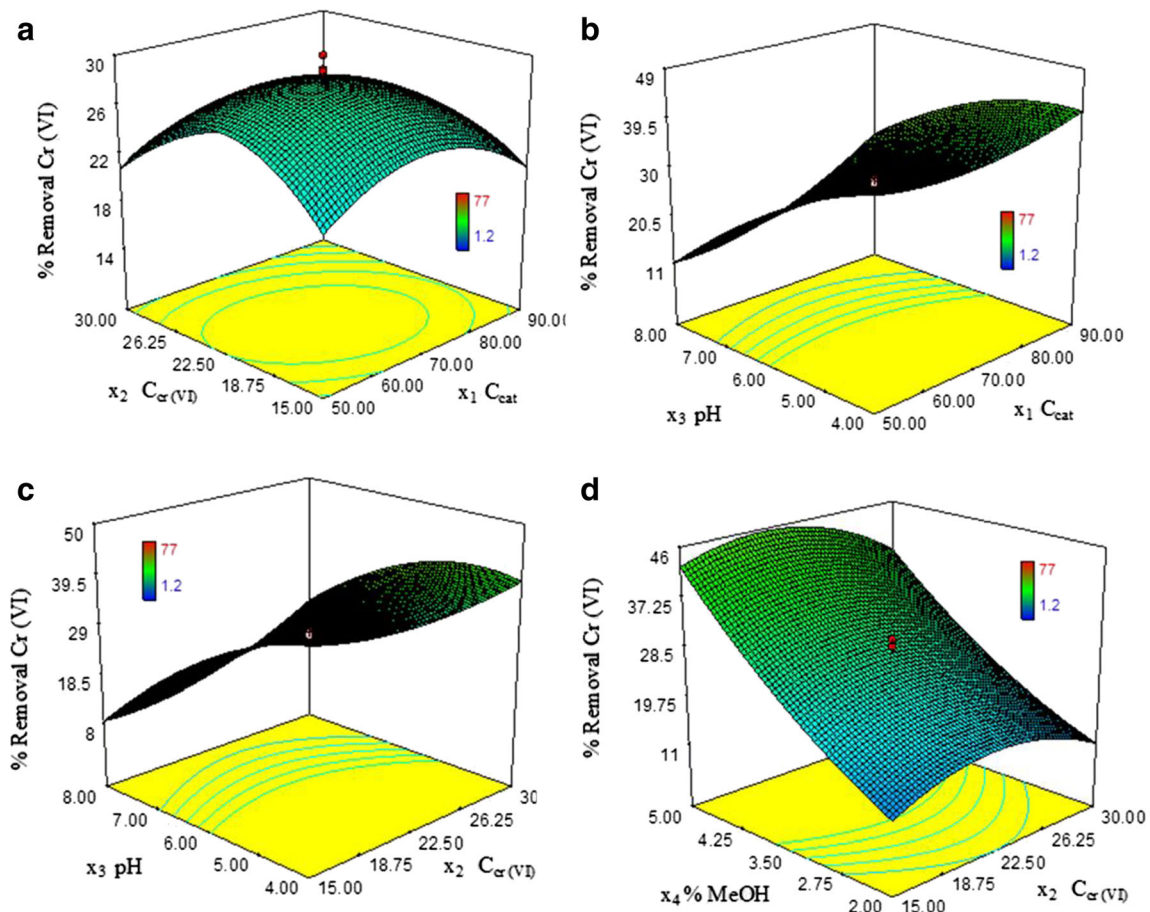
Fig. 5 Three-dimensional response surface plots using RSM for Cr(VI) photocatalytic reduction: **a** Cr(VI) concentration vs. catalyst's concentration, **b** pH vs. catalyst's concentration, **c** pH vs. Cr(VI) concentration, and **d** % (v/v) methanol (MeOH) vs. Cr(VI) concentration

can be observed that the removal rate on PC/TiO$_2$ remained at about 70 % after five recycling with 1-h adsorption in the dark and consecutive 1-h photocatalytic reduction under UV–Vis irradiation in each cycle, indicating that PC/TiO$_2$ could be considered stable under the studied experimental conditions.
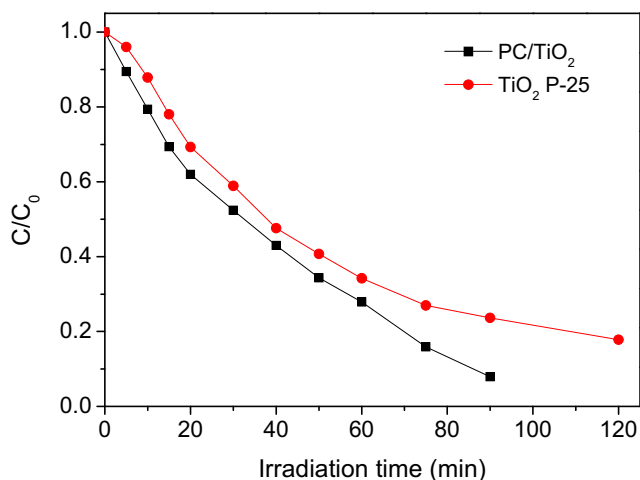

Fig. 6 Kinetics of Cr(VI) photocatalytic reduction under optimized conditions ($C_{cat} = 55$ mg L^{-1}, $C_{Cr(VI)} = 20$ mg L^{-1}, pH = 4, % (v/v) methanol = 5 %)
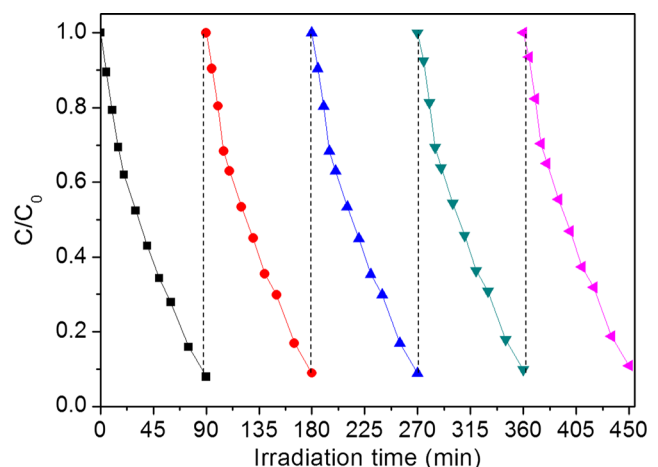

Fig. 7 Reusability of PC/TiO$_2$ catalyst after five photocatalytic reduction cycles of Cr(VI) ($C_{cat} = 55$ mg L^{-1}, $C_{Cr(VI)} = 20$ mg L^{-1}, pH = 4, % (v/v) methanol = 5 %)

Conclusions

The photocatalytic reduction kinetics of Cr(VI) in the presence of pyrolytic char/TiO$_2$ nanocomposite material were investigated in detail. Response surface methodology based on a CCD was used successfully to optimize significant operational parameters to maximize Cr(VI) removal. All four parameters studied, i.e., concentration of Cr(VI) and catalyst, pH, and the concentration of methanol, presented significant effects on the total efficiency. However, pH and % methanol content were by far the more crucial parameters with pH = 4 and 5 % (v/v) being the optimized conditions. Immobilization of TiO$_2$ nanoparticles on tire pyrolytic char showed an increased efficiency on the photocatalytic reduction of Cr(VI) due to the decreased recombination rate of photogenerated e$^-$–h$^+$ pairs. The catalyst shows no significant loss of their catalytic activity after five consecutive catalyst cycles. The results obtained indicate that the RSM is a powerful tool for optimizing the operational conditions of the reduction of Cr(VI) in the presence of methanol.

References

Antonopoulou M, Konstantinou I (2013) Optimization and modeling of the photocatalytic degradation of the insect repellent DEET in aqueous TiO$_2$ suspensions. Clean Soil Air Water 41(6):593–600

Antonopoulou M, Konstantinou I (2015) Photocatalytic degradation of pentachlorophenol by visible light N-F-TiO$_2$ in the presence of oxalate ions: optimization, modeling and scavenging studies. Environ Sci Pollut Res 22:9438–9448

Antonopoulou M, Giannakas A, Konstantinou I (2012) Simultaneous photocatalytic reduction of Cr(VI) and oxidation of benzoic acid in aqueous N-F-co-doped TiO$_2$ suspensions: optimization and modeling using the response surface methodology. Int J Photoenergy. doi:10.1155/2012/520123

Barrera-Díaz CE, Lugo-Lugo V, Bilyeu B (2012) A review of chemical, electrochemical and biological methods for aqueous Cr(VI) reduction. J Hazard Mater 223–224:1–12

Chen SF, Cao GY (2005) Study on the photocatalytic reduction of dichromate and photocatalytic oxidation of dichlorvos. Chemosphere 60:1308–1315

Cheng Q, Wang C, Doudrick K, Chana CK (2015) Hexavalent chromium removal using metal oxide photocatalysts. Appl Catal B Environ 176–177:740–748

Chong MN, Jin B, Chow CWK, Saint C (2010) Recent developments in photocatalytic water treatment technology: a review. Water Res 44:2997–3027

Fathinia M, Khataee AR, Zarei M, Aber S (2010) Comparative photocatalytic degradation of two dyes on immobilized TiO$_2$ nanoparticles: effect of dye molecular structure and response surface approach. J Mol Catal A Chem 333(1–2):73–84

Fu X, Yang H, Lu G, Tu Y, Wu J (2015) Improved performance of surface functionalized TiO$_2$/activated carbon for adsorption–photocatalytic reduction of Cr(VI) in aqueous solution. Mater Sci Semicond Proces 39:362–370

Giannakas AE, Antonopoulou M, Deligiannakis Y, Konstantinou I (2013) Preparation, characterization of N–I co-doped TiO$_2$ and catalytic performance toward simultaneous Cr(VI) reduction and benzoic acid oxidation. Appl Catal B Environ 140–141:636–645

Giannakas AE, Antonopoulou M, Daikopoulos C, Deligiannakis Y, Konstantinou I (2016) Characterization and catalytic performance of B-doped, B-N co-doped and B-N-F tri-doped TiO$_2$ towards simultaneous Cr(VI) reduction and benzoic acid oxidation. Appl Catal B Environ 184:44–54

Hawley EL, Deeb RA, Kavanaugh MC, Jacobs JRG (2004) Treatment technologies for chromium(VI). In: Guertin J, Jacobs JA, Avakian CP (eds) Chromium(VI) handbook. CRC Press, Boca Raton, pp 275–310

Jacobs JA, Testa SM (2004) Overview of chromium(VI) in the environment: backround and history. In: Guertin J, Jacobs JA, Avakian CP (eds) Chromium(VI) handbook. CRC Press, Boca Raton, pp 1–20

Jiang G, Lin Z, Chen C, Zhu L, Chang Q, Wang N, Wei W, Tang H (2011) TiO$_2$ nanoparticles assembled on graphene oxide nanosheets with high photocatalytic activity for removal of pollutants. Carbon 49:2693–2701

Konstantinou IK, Albanis TA (2003) Photocatalytic transformation of pesticides in aqueous TiO$_2$ suspensions using artificial and solar light. Appl Catal B Environ 42:319–335

Konstantinou IK, Albanis TA (2004) TiO$_2$-assisted photocatalytic degradation of azo dyes in aqueous solution: kinetic and mechanistic investigations. Appl Catal B Environ 49:1–14

Ku Y, Jung IL (2001) photocatalytic reduction of Cr(VI) in aqueous solutions by UV irradiation in the presence of titanium dioxide. Water Res 35:135–142

Leary R, Westwood A (2011) Carbonaceous nanomaterials for the enhancement of TiO$_2$ photocatalysis. Carbon 49:741–772

Lim TT, Yap PS, Srinivasan M, Fane AG (2011) TiO$_2$/AC composites for synergistic adsorption-photocatalysis processes: present challenges and further developments for water treatment and reclamation. Crit Rev Environ Sci Technol 41:1173–1230

Lin WY, Wei C, Rajeshwar K (1993) Photocatalytic reduction and immobilization of hexavalent chromium at titanium dioxide in aqueous basic media. J Electrochem Soc 140:2477–2482

Liu W, Ni J, Yin X (2014) Synergy of photocatalysis and adsorption for simultaneous removal of Cr(VI) and Cr(III) with TiO$_2$ and titanate nanotubes. Water Res 53:12–25

Ma M, Guo W, Yang Z, Huang S, Wang G (2015) Preparation and photocatalytic activity of TiO$_2$/fine char for removal of rhodamine B. J Nanomat Article ID 538275, 5 pages

Machado TC, Lansarin MA, Matte N (2014) Reduction of hexavalent chromium: photocatalysis and photochemistry and their application in wastewater remediation. Water Sci Technol 70:55–61

Makrigianni V, Giannakas A, Daikopoulos C, Deligiannakis Y, Konstantinou I (2015) Preparation, characterization and photocatalytic performance of pyrolytic-tire-char/TiO$_2$ composites, toward phenol oxidation in aqueous solutions. Appl Catal B Environ 174–175:244–252

Mukherjee K, Saha R, Ghosh A, Saha B (2013) Chromium removal technologies. Res Chem Intermed 39:2267–2286

Owlad M, Aroua MK, Daud WAW, Baroutian S (2008) Removal of hexavalent chromium-contaminated water and wastewater: a review. Water Air Soil Pollut 200:59–77

Pi L, Jiang R, Zhou W, Zhu H, Xiao W, Wang D, Mao X (2015) g-C3N4 modified biochar as an adsorptive and photocatalytic material for decontamination of aqueous organic pollutants. Appl Surf Sci 358:231–239

Rezaee A, Rangkooy H, Khavanin A, Jonidi Jafari A (2014) High photocatalytic decomposition of the air pollutant formaldehyde using nano-ZnO on bone char. Environ Chem Lett 12:353–357

Shaham-Waldmann N, Paz Y (2013) Beyond charge separation: the effect of coupling between titanium dioxide and CNTs on the adsorption and photocatalytic reduction of Cr(VI). Chem Eng J 231:49–58

Tan T, Beydoun D, Amal R (2003) Effects of organic hole scavengers on the photocatalytic reduction of selenium anions. J Photochem Photobiol A Chem 159:273–280

Tandon RK, Crisdp PY, Ellis J, Baker RS (1984) Effect of pH on chromium(VI) species in solution. Talanta 31:227–228

Vaez M, Moghaddam AZ, Alijani S (2012) Optimization and modeling of photocatalytic degradation of azo dye using a response surface methodology (RSM) based on the central composite design with immobilized titania nanoparticles. Ind Eng Chem Res 51: 4199–4207

Wang SL, Chen CC, Tzou YM, Hsu CL, Chen JH, Lin CF (2009) A mechanism study of light-induced Cr(VI) reduction in an acidic solution. J Hazard Mater 164(1):223–228

Wang C, Cao M, Wang P, Ao Y, Hou J, Qian J (2014) Preparation of graphene–carbon nanotube–TiO2 composites with enhanced photocatalytic activity for the removal of dye and Cr (VI). Appl Catal A Gen 473:83–89

Yue D, Qian X, Zhao Y (2015) Photocatalytic remediation of ionic pollutant. Sci Bull 60:1791–1806

Zhao D, Sheng G, Chen C, Wang X (2012) Enhanced photocatalytic degradation of methylene blue under visible irradiation on graphene@TiO2 dyade structure. Appl Catal B Environ 111–112: 303–308

Zhao Y, Zhao D, Chen C, Wang X (2013a) Enhanced photo-reduction and removal of Cr(VI) on reduced grapheme oxide decorated with TiO2 nanoparticles. J Colloid Interface Sci 405:211–217

Zhao D, Yang X, Chen C, Wang X (2013b) Enhanced photocatalytic degradation of methylene blue on multiwalled carbon nanotubes–TiO2. J Colloid Interface Sci 398:234–239